JAAS

Accepted Manuscript

This is an *Accepted Manuscript*, which has been through the Royal Society of Chemistry peer review process and has been accepted for publication.

Accepted Manuscripts are published online shortly after acceptance, before technical editing, formatting and proof reading. Using this free service, authors can make their results available to the community, in citable form, before we publish the edited article. We will replace this *Accepted Manuscript* with the edited and formatted *Advance Article* as soon as it is available.

You can find more information about *Accepted Manuscripts* in the Information for Authors.

Please note that technical editing may introduce minor changes to the text and/or graphics, which may alter content. The journal's standard Terms & Conditions and the Ethical guidelines still apply. In no event shall the Royal Society of Chemistry be held responsible for any errors or omissions in this *Accepted Manuscript* or any consequences arising from the use of any information it contains.

ROYAL SOCIETY OF CHEMISTRY

www.rsc.org/jaas

Effects of ionization potential of an element and boiling point of the corresponding oxide on the sensitivity of ICP-MS

Koon-Sing Ho[‡], Wan-Waan Lee, and Wing-Tat Chan*

Department of Chemistry, The University of Hong Kong, Pokfulam Road, Hong Kong.

[‡] current address: Department of Chemistry, Hong Kong Baptist University, Waterloo Road, Hong Kong.

Email address: wtchan@hku.hk; Tel: +852-2859-2156; Fax: +852-2857-1586.

Abstract

In this study, the sampling depth profiles of 19 elements in aqueous solution were obtained. The selected elements cover a wide range of atomic weight, ionization potentials, and oxide boiling points. The sampling position of maximum ICP-MS sensitivity of the elements depends on the boiling point of the corresponding oxide and the ionization potential of the elements. The boiling point determines the position in the ICP where significant vaporization of the dried aerosols occurs. In general, the peak position increases as the oxide boiling point of an element increases. However, the peak position for elements of high ionization potential and low oxide boiling point is downstream of the point of complete vaporization. The combined effect of analyte ionization potential and oxide boiling point on the optimized sampling position is illustrated by the linear plot of the difference in the temperature for significant ionization of an element and the boiling point of the corresponding oxide *versus* the oxide boiling point. The sampling depth profiles of single-particle ICP-MS of Au and ZrO_2 nanoparticles and the corresponding standard solution are of similar shape. The peak maximum of the sampling depth profiles shifts to a slightly higher position for the refractory ZrO_2 and large Au nanoparticles. The duration of particle vaporization for the nanoparticles becomes a significant factor in determining the peak position.

1. Introduction

Inductively coupled plasma (ICP) is one of the most commonly used atomization and ionization sources in mass spectrometry (MS). Because of the low limits of detection, high selectivity, and large linear dynamic range, ICP-MS has become the predominant technique for trace or ultra-trace elemental analysis of industrial, biological, environmental, pharmaceutical, and forensic samples [1,2].

Samples in the form of aqueous solution are typically introduced into the ICP as fine aerosols using solution nebulization. The aerosols undergo desolvation in the ICP until dried particles of the analyte and the matrix remain. The dried aerosols, which are effectively nanoparticles, are further heated up by the ICP and vaporize at high rate when the boiling point of the particle is reached [3-5]. Molecules of the analyte released from the particles are subsequently atomized. Some of the analyte atoms are ionized and a small fraction of the ions is sampled into the mass spectrometer for detection.

In a study by Olesik [6], single droplets of Y standard solution of diameter of 60 μm and concentration of hundreds of μg/L were introduced into the ICP using monodisperse dried microparticulate injection (MDMI). The diameter of the dried aerosols was of the order of hundred nanometers. The vaporization and atomization processes of the relatively large dried aerosols were shown to be relatively fast compared to the ionization process. The maxima of optical emission intensity of YO, Y, and Y^+ occurred at 40, 60, and 210 μs after the first measurable emission of YO, respectively. The time required for vaporization, atomization, and ionization were, therefore, 40, 20, and 150 μs, respectively. The time required for vaporization and atomization was approximately 60 μs. The 60-μm aerosols generated by MDMI is

significantly larger than the aerosols that are generated using nebulizer / spray chamber for sample introduction in typical ICP-MS measurement. The diameter of the sample aerosols that can reach the ICP are no more than a few micrometers [1]. The diameter of the dried aerosols is estimated to be of the order of 10 nm or less. Therefore, the time for complete vaporization and atomization of the dried aerosols is expected to be much less than 60 μs and should not be a limiting factor that determines the sampling position for maximum ICP-MS sensitivity.

Optimization of the sampling position for maximum sensitivity have been reported by many research groups over the years [7-17]. In general, volatility of the analyte was found to be the main controlling factor. Low-boiling alkali elements peak at low positions of the ICP and elements of refractory oxides peak at higher positions [7-9]. Ionization potential was shown to have little effects on the sampling position [10]. Among the test elements (B, Zn, Cs, Ba, Sm, and Pb), Zn has the highest ionization potential but the optimal sampling position was the lowest. These studies were, however, based on relatively small sets of elements. Only the main controlling factor, *i.e.*, analyte vaporization, can be identified from the small sets of data. The contribution of additional controlling factors, if any, is generally not discernible. In addition, the spatial resolution of the sampling depth profile was typically 0.5 mm or larger, insufficient to pinpoint the maximum positions for in-depth investigation of the controlling factors. In Olesik's study [6], analyte vaporization and ionization were shown to be the main factors for ion production. We propose that the critical parameters that determine the sampling position for maximum ICP-MS sensitivity are the position of complete vaporization of the dried aerosols and the position of significant ionization of the analyte atoms. These two positions are determined by the boiling point of the dried aerosols [18], and the ionization potential of the

element [19], respectively. A comprehensive study of the effects of ionization potential of the element and boiling point of the corresponding dried aerosols on the position of maximum sensitivity would be useful for optimization of ICP-MS sampling depth, especially for single-particle inductively coupled plasma-mass spectrometry (SP-ICP-MS) measurement of relatively large nanoparticles and biological cells.

In this study, the sampling depth profiles of 19 elements in aqueous solution were used to delineate the effects of particle vaporization and analyte ionization on the peak position and the shape of the profiles. The elements were selected to cover a wide range of atomic weight, ionization potential, and oxide boiling point (Table 1). The mass range of the elements is 7 to 208 Da, covering nearly 90% of the mass range accessible by ICP-MS. The selected elements also represent a wide range of ionization potential (520 to 950 kJ/mol) and oxide boiling point (740 to 4600 K) [20-22]. Since the dried particles of the analyte are mainly the corresponding oxide species of the element [23], the vaporization of the oxide, instead of the element, will be the focus of this study. The ionization potential of the elements and the boiling point of the corresponding oxides are correlated with the peak position and the shape of the sampling depth profiles. In addition, the study is extended to single-particle ICP-MS measurement of Au and ZrO_2 nanoparticles.

2. Experimental

2.1 Chemicals and solutions

Stock solutions of 1000 μg/mL of the 19 test elements, except for V and As, were prepared separately by dissolving the corresponding analytical grade nitrate salts (Fluka and Riedel-de Haen, Seelze, Germany) in 1% (v/v) nitric acid (Ultra-pure grade, Fluka, Seelze, Germany). The stocks were stored in polyethylene bottles. Stock

solutions of 10000 µg/mL of V and As were purchased from Sigma-Aldrich Corporation (MO, USA). Single-element and multi-element standard solutions of elements of the desired concentrations were prepared from the corresponding stock solutions by dilution in deionized water prior to ICP-MS measurement. Li of 100 µg/L, Al and As of 25 µg/L each, and a multi-element standard solution containing 10 µg/L each of the remaining 16 elements were used in the depth profile measurement. The concentrations of the analytes were selected to give signal-to-noise ratio of at least 10. The peak position of an element is independent of the analyte concentration (Section 3.1).

In single-particle ICP-MS measurement, suspensions of Au (nominal diameter of 150 nm and 250 nm, British Biocell International, Cardiff, UK) and ZrO_2 (nanopowder, < 100 nm (TEM), Sigma-Aldrich Corporation, MO, USA) nanoparticles were used. The average diameter of the ZrO_2 nanoparticles was 80 nm as determined using dynamic light scattering (3000HS_A Zetasizer, Malvern Instruments Ltd., Malvern, UK). Suspensions of the nanoparticle were freshly prepared and diluted to number density of approximately 10^4 /mL using deionized water prior to SP-ICP-MS measurement.

2.2 ICP-MS measurement

Spectrum (peak hopping) mode of the quadrupole-based inductively coupled plasma mass spectrometer (Agilent 7500a, Agilent Technologies, CA, USA) was used in this study. Typical operating parameters of the ICP-MS are listed in Table 2. The ICP forward power was 1200 W. The diameter of injector of the ICP torch was 2.5 mm. Relatively high central channel gas flow rate of 1.25 L/min was selected so that the positions of maximum sensitivity of all test elements were located within the usable

sampling depth of 3 mm or above. ICP-MS intensity of each element was measured at sampling depth of 3.0 to 7.0 mm, in 0.1 mm increments. The spatial resolution of sampling depth profile of 0.1 mm is sufficient to pinpoint the maximum positions of the elements.

In single-particle measurement, time-resolved analysis (TRA) mode of the ICP-MS was used. The operating parameters are also listed in Table 2. The minimum dwell time of 10 ms was used. Sample uptake rate of 0.4 mL/min and number density of the nanoparticle in the sample suspension of approximately 10^4 /mL were used to give appearance rate of the ICP-MS intensity spikes of approximately 2 Hz. For the comparison between the sampling depth profiles of the nanoparticles and aqueous standard solution, the corresponding aqueous solutions were measured using the same ICP-MS operating parameters for single-particle measurement, except for the use of spectrum mode of dwell time of 100 ms.

Before each experiment, the ICP-MS was tuned using a multi-element standard solution of 10 µg/L each of Li, Y, Co, Ce, and Tl for consistent sensitivity of ^{7}Li, ^{89}Y, and ^{205}Tl, and minimum levels of doubly-charged ions and oxide species of ^{140}Ce.

3. Results and discussion

In the following sections, the combined effects of the boiling point of the dried aerosols and the ionization potential of the element on the peak position and the shape of the sampling depth profiles will be discussed. First, the size (mass) of the dried aerosols will be shown to have no effects on the peak position in the next section. The finding allows flexible selection of standard concentration to give adequate signal-to-noise ratio (typically 100) for the depth profile measurement.

3.1 Effect of the size of the dried aerosols

The vaporization process of dried aerosols of diameter of 10^2 nm is relatively fast, compared to other signal production processes such as desolvation of the aerosols and ionization of the elements [6]. The dried aerosols produced by nebulization of aqueous solutions is much smaller, typically of diameter of a few nanometers, and the time required for complete vaporization of the particles is expected to be negligible. The optimal sampling position should, therefore, be independent of the size of the dried aerosols. In Table 3, the positions of maximum sensitivity of Ce are indeed independent of the concentration of Ce over 4 orders of magnitude (1 – 10000 μg/L). The diameter of the dried aerosols were approximately 1 to 25 nm (Table 3), assuming average aerosol diameter of 2 μm [1] and Ce_2O_3 density of 6.20 g/cm^3 [22]. Since the aerosol diameter was not measured, the estimated dried aerosol diameter is not exact. However, the size of the dried aerosols should fall in the range of nanoparticles (diameter 1 to 100 nm). Cerium was selected because of the relatively high boiling point of the refractory cerium oxide (4000 K) and modest ionization potential of Ce (530 kJ/mol). The high boiling point will accentuate the effect of the vaporization process because vaporization rate reduces as boiling point increases [3-5]. The relatively low ionization potential will have little effect on the peak position of the sampling depth profile (Section 3.3). In a similar experiment using Cd of concentration of 10 – 10000 μg/L, the position of maximum sensitivity was also independent of the concentration of the element [17]. Cd is different from Ce in that the boiling point of the oxide of Cd (1800 K) is much lower, while the ionization potential is higher (870 kJ/mol). The peak position is mainly determined by the degree of ionization of Cd (Section 3.3). For both cases, the sampling position for maximum ICP-MS sensitivity of an element is independent of the analyte concentration. The vaporization time of the dried aerosols, therefore, must be

relatively short and the position where particle vaporization begins is approximately the position of complete particle vaporization for the small particles (<100 nm). Since the time scale of the atomization of analyte molecules is shorter than that of the vaporization of dried particles [6], the atomization process is expected to have even less effect on the position of maximum sensitivity and will not be further considered.

3.2 Effect of the boiling point of the dried aerosols

The peak position of the sampling depth profile depends critically on the volatility of the dried aerosols (residue) of the sample solution. Low-boiling residues peak at lower position of the ICP, while high-boiling residue peak at higher position [7-9]. The boiling point of the residue presumably determines the position in the ICP where significant vaporization of the residue occurs. Another parameter related to particle vaporization is the particle size. However, as shown in the last section, the particle size has little effects on the peak position for the size range of typical dried aerosols. The effects of the boiling point of the dried aerosols on the peak position will be examined in the following paragraphs.

Typical sampling depth profiles of four elements (Pb, Ni, Cr, and Ce) are shown in Figure 1. The oxides represent the full range of volatility of the oxides studied (Table 1). The sampling depth profiles of the remaining 15 elements were shown in Figure S1. The peak positions of the elements are given in Table 4. The position of maximum sensitivity ranges from 3.8 to 6.1 mm. The positions generally increase as the ICP forward power decreases (Figure S2). The boiling points of the elements and the corresponding oxides are plotted against the peak positions in Figure 2. The peak position generally increases with the boiling points, in agreement with the literatures

[7-9]. The boiling points of the oxides, however, show stronger correlation with the peak position (Figure 2a). The dried aerosols of the aqueous solution are, therefore, likely the corresponding oxides of the elements [23], which is in agreement with the observation of thermal study of decomposition of metal nitrate at high temperature [24-27]. The peak position also increases with the melting point of the oxide (Figure S3). However, the correlation is not as strong as that of the oxide boiling point. As soon as a solid particle melts, vapor pressure is developed over the molten droplet. The vapor pressure increases quickly with temperature [28]. At the peak position of the sampling depth profile, the particle is significantly, if not completely, vaporized [29]. The peak position, therefore, correlates better with the boiling point rather than the melting point of the oxide.

In Figure 2a, the peak position of the sampling depth profile generally correlates with the boiling points of the oxides except for the low-boiling As, Cd, and Pb. The sampling depth profiles of the volatile oxides generally rise gently at low sampling position before the peak maximum (Li, Ni, Cu, Zn, Cd, and Pb in Figures 1 and S1). The gentle rising slope of the sampling depth profile is probably a result of the opposing effects of progressive increase in the degree of ionization and diffusion loss of the analyte atoms as the atom plume moves up the ICP. Cd and Pb show the same pattern of sampling depth profiles but the peak position of the elements is higher than expected (Figure 2a), probably because the ionization potential of the elements are relatively high (Section 3.3). The low-boiling arsenic oxide shows relatively fast rising slope yet the peak position is also higher than expected (Figure 2a), probably because of combined effects of high oxide bond energy of arsenic oxide and very high ionization potential of As (Section 3.3). The combined effects of oxide boiling

point and the degree of ionization on the peak position of the sampling depth profiles will be discussed in the next section.

The relatively fast rising slope in the sampling depth profiles of the remaining elements (Figures 1 and S1) is due to low degree of vaporization of the high-boiling oxides at low sampling positions. The degree of vaporization increases quickly as the sampling depth and thus the plasma temperature increase [3-5,30]. The declining slope of the sampling-depth profiles is similar for all elements, which is mainly dependent on diffusion loss of the analyte ions [31].

3.3 Combined effect of the ionization potential and the boiling point

ICP-MS intensity is directly related to the degree of ionization of the analyte, which is dependent on the ionization potential (IP) and the ionization temperature of the ICP. The ionization potentials of the elements are plotted against the positions of maximum sensitivity of the sampling depth profiles in Figure 3. There is no obvious relationship between the peak position of the sampling depth profiles and the ionization potential of the elements alone, which agrees with the observation in the literatures [10]. The lack of correlation of IP with the peak position in Figure 3 and the outlier of the low-boiling As, Cd, and Pb in the plot of oxide boiling point *versus* peak position in Figure 2a point to the necessity for the consideration of the combined effects of particle vaporization and analyte ionization.

As discussed in Section 3.1, the oxides vaporize quickly at their respective boiling points and the ICP temperature at which the particles are completely vaporized is approximately the boiling point of the particles. For the volatile oxides, the degree of ionization will likely be very low at this position. The degree of ionization of the test

elements at the boiling point of the corresponding oxides are calculated using Saha equation [19]. The partition functions were calculated according to the method by de Galan *et al.* [32] and the electron number density of the ICP was assumed to be 10^{15} /cm^3 [33]. Figure 4 shows that the degree of ionization is low for elements of volatile oxides but relatively high ionization potential (Ni, Cu, Zn, as well as As, Cd, and Pb). These elements are expected to peak at position higher than the position where vaporization of the dried aerosols has already completed. In contrast, the degree of ionization at the oxide boiling point is approximately 100% for elements of refractory oxides of boiling point $\geq$ 4000 K (Y, Zr, La, Ce, and Gd) and $\geq$ 90% for elements of oxide boiling points > 3000 K (Ti, Al, Cr, Sr and V). These elements will have the maximum sensitivity when the dried aerosols reach the boiling point and are fully vaporized and highly ionized in the ICP. The position of maximum ICP-MS sensitivity, therefore, depends on the boiling point of the oxides for high-boiling oxides or the difference between the boiling point and the temperature for high degree of ionization for elements of high ionization potential and low-boiling oxides.

At a typical ICP ionization temperature of approximately 9000 K, elements of ionization potential of 870 kJ/mol or below are more than 80% ionized [34]. In the following study, the temperature for 80% ionization of the test elements (T_{80}) is calculated (Table S2). The difference in the position of 80% ionization of the element and the position of complete vaporization is represented by the difference in T_{80} and the boiling point of the corresponding oxide in Figure 5, assuming linear relationship of ICP temperature and ICP axial position. ICP temperature varies linearly with sampling depth over a larger range of axial position from -5 to 10 mm [5,35]. The range of sampling depth in this study is relatively narrow, from 3 to 7 mm above the load coil. Therefore, the plasma temperature profile is probably linear. The

difference in temperature is linearly and negatively correlated with the oxide boiling point (Figure 5). Ionization of the elements plays an important role in governing the sampling position for maximum ICP-MS sensitivity of an element. Elements of high ionization potential and volatile oxides will have the position of maximum sensitivity farther away from the position of complete vaporization, while elements of refractory oxide tend to have the peak position coincide with the position of complete vaporization. The negative difference in temperature in Figure 5 signifies that the boiling point of the oxides is higher than the required temperature for significant analyte ionization. The elements are expected to be highly ionized once the boiling point of the oxides is reached and the vaporization is completed.

The calculated temperature differences of Mg, Zn, and Cd are larger than expected in Figure 5. Cd and Zn have relatively high ionization potential but the oxide boiling points are very low (Table 1). The calculated temperature difference is 3700 and 3900 K for Zn and Cd, respectively (Table S2). The atom plume must transverse a few mm in the ICP from the point of complete vaporization to the point of 80% ionization. However, significant loss of analyte atoms by diffusion is expected as the atom plume moves up the ICP over a long distance. The position of maximum sensitivity is, therefore, lower than expected. In other words, the degree of ionization at the peak position is likely much lower than 80%. For the case of Mg, the calculated temperature difference is relatively modest (800 K). The discrepancy from the linear relationship in Figure 5 is likely due to significant loss of the low atomic mass Mg atoms by diffusion once the dried aerosols are completely vaporized. The assumption of 80% ionization at the position of maximum sensitivity for the three elements in the calculation leads to overestimation of the temperature differences.

3.4 Sampling depth for SP-ICP-MS

The vaporization characteristics of nanoparticles in the ICP was well-investigated in the literatures using laser ablated materials [18,36-38] and dried particles generated by MDMI or piezoelectical microdroplet generator [29,39-42]. The time for complete vaporization of nanoparticles of diameter of >100 nm is of the order of tens of microseconds [6], significantly longer than that of the dried aerosols of the aqueous solutions in the previous sections. The time required for complete vaporization of the nanoparticles may have significant effects on the position of maximum sensitivity. Some of the large particles were, in fact, incompletely vaporized in the ICP [30,36]. In this study, the sampling depth profiles of nanoparticles of Au (diameter of 150 nm and 250 nm) and ZrO_2 (diameter of 80 nm) and the corresponding standard solutions are compared to determine the effects of particle vaporization on the sampling depth profiles (Figure 6). The nanoparticles are selected to represent two combinations of ionization potential and boiling point. Au has high ionization potential (890 kJ/mol) and moderate boiling point (3100 K), while Zr has moderate ionization potential (640 kJ/mol) and ZrO_2 has relatively high boiling point (4600 K). The discrete test particles were measured using SP-ICP-MS [30,43-46]. The peak maximum of the log-normal ICP-MS spike intensity distribution was used as the average intensity of the discrete particles at each sampling depth.

The sampling depth profiles of Au standard solution (concentration of 10 µg/L) and the 150-nm Au nanoparticles of are nearly identical (Figure 6a). The peak of the sampling depth profile, however, shifts to a higher position for the 250-nm Au nanoparticles. The longer vaporization time of the large Au nanoparticles delays the occurrence of the peak. For the 80-nm ZrO_2 nanoparticle, delay in the occurrence of the peak compared to the standard solution (10 µg/L) is also observed (Figure 6b).

The delay in the occurrence of the peak in the sampling depth profile for elements of moderate to high boiling points highlights the significance of particle vaporization in SP-ICP-MS measurement. The high ionization potential of Au did not determine the peak position for the large nanoparticles, in contrast to the cases of dried aerosols in Section 3.3.

It is interesting to note that the shift in peak position of the 250-nm gold and ZrO_2 nanoparticles *versus* the respective aqueous solutions is relatively small, approximately 0.5 mm only (Figure 6). The sampling depth profiles of aqueous solutions can be used as a quick guide for the selection of the sampling depth position for SP-ICP-MS for maximum sensitivity. An advantage of SP-ICP-MS measurement at the peak position is that systematic errors by solution calibration due to the varying sampling depth profiles *versus* particle size are minimal at the peak. Relatively accurate calibration using standard solution for particle size determination is possible at the optimized sampling position of the standard solution.

4. Conclusions

The ionization potential of an element and the boiling point of the corresponding oxide are the two major factors that determine the shape of ICP-MS sampling depth profile and the peak position of the profile. The peak of the sampling depth profiles for elements of volatile oxides generally occurs at low sampling positions, except for those elements of high ionization potential, of which the peak occurs at higher positions where significant ionization occurs. The peak of elements of refractory oxides generally occurs at high sampling positions, at the position of complete vaporization of the oxides. The optimized sampling position, therefore, depends on

the boiling point of the oxides for high-boiling oxides or the difference between the boiling point and the temperature for high degree of ionization for elements of high ionization potential and low-boiling oxides. For the large discrete nanoparticles, the peak of the sampling depth profile shifts downstream because of the longer duration for complete vaporization of the particles. Nonetheless, the profile of aqueous solution can be used as a guide for the selection of the sampling depth of SP-ICP-MS.

Acknowledgements

This work was supported by a grant from the Research Grant Council of the Hong Kong Special Administrative Region, China (Project No. 17300414) and the Seed Funding Programme for Basic Research of The University of Hong Kong.

References

1. A. Montaser, ed., *Inductively coupled plasma mass spectrometry*, J. Wiley, New York, 1998.
2. S. J. Hill, ed., *Inductively coupled plasma spectrometry and its applications*, Blackwell Publishing Ltd, Oxford, 2006.
3. J. A. Horner and G. M. Hieftje, *Spectrochimica Acta Part B-Atomic Spectroscopy*, 1998, **53**, 1235-1259.
4. J. A. Horner, S. A. Lehn and G. M. Hieftje, *Spectrochimica Acta Part B-Atomic Spectroscopy*, 2002, **57**, 1025-1042.
5. J. A. Horner, G. C.-Y. Chan, S. A. Lehn and G. M. Hieftje, *Spectrochimica Acta Part B-Atomic Spectroscopy*, 2008, **63**, 217-233.
6. J. W. Olesik, *Applied Spectroscopy*, 1997, **51**, A158-A175.
7. M. M. Fraser and D. Beauchemin, *Spectrochimica Acta Part B-Atomic Spectroscopy*, 2000, **55**, 1705-1731.

8. M. M. Fraser and D. Beauchemin, *Spectrochimica Acta Part B-Atomic Spectroscopy*, 2001, **56**, 2479-2495.

9. G. Horlick, S. H. Tan, M. A. Vaughan and C. A. Rose, *Spectrochimica Acta Part B-Atomic Spectroscopy*, 1985, **40**, 1555-1572.

10. S. E. Long and R. M. Brown, *Analyst*, 1986, **111**, 901-906.

11. S. H. Tan and G. Horlick, *Applied Spectroscopy*, 1986, **40**, 445-460.

12. M. A. Vaughan and G. Horlick, *Applied Spectroscopy*, 1986, **40**, 434-445.

13. A. L. Gray and J. G. Williams, *Journal of Analytical Atomic Spectrometry*, 1987, **2**, 599-606.

14. H. P. Longerich, B. J. Fryer, D. F. Strong and C. J. Kantipuly, *Spectrochimica Acta Part B-Atomic Spectroscopy*, 1987, **42**, 75-92.

15. S. H. Tan and G. Horlick, *Journal of Analytical Atomic Spectrometry*, 1987, **2**, 745-763.

16. M. A. Vaughan, G. Horlick and S. H. Tan, *Journal of Analytical Atomic Spectrometry*, 1987, **2**, 765-772.

17. G. X. Zhu and R. F. Browner, *Applied Spectroscopy*, 1987, **41**, 349-359.

18. L. Flamigni, J. Koch and D. Günther, *Spectrochimica Acta Part B: Atomic Spectroscopy*, 2012, **76**, 70-76.

19. H. Niu and R. S. Houk, *Spectrochimica Acta Part B-Atomic Spectroscopy*, 1996, **51**, 779-815.

20. O. Knacke, O. Kubaschewski and K. Hesselmann, eds., *Thermochemical properties of inorganic substances*, Springer-Verlag, Berlin, 1991.

21. C. L. Yaws, *Handbook of thermodynamic diagrams. vol. 4, Inorganic compounds and elements*, Gulf Pub. Co., Houston, 1996.

22. D. R. Lide, ed., *CRC handbook of chemistry and physics*, 79th edn., CRC Press LLC, Boca Raton, 1998.

23. E. Poussel, J. M. Mermet and D. Deruaz, *Journal of Analytical Atomic Spectrometry*, 1994, **9**, 61-66.

24. J. G. Jackson, A. Novichikhin, R. W. Fonseca and J. A. Holcombe, *Spectrochimica Acta Part B-Atomic Spectroscopy*, 1995, **50**, 1423-1426.

25. J. G. Jackson, R. W. Fonseca and J. A. Holcombe, *Spectrochimica Acta Part B-Atomic Spectroscopy*, 1995, **50**, 1449-1457.

26. B. V. Lvov, *Mikrochimica Acta*, 1991, **2**, 299-308.

27. B. V. Lvov and A. V. Novichikhin, *Spectrochimica Acta Part B-Atomic Spectroscopy*, 1995, **50**, 1427-1448.

28. C. L. Yaws, *Handbook of vapor pressure. vol. 4, Inorganic compounds and elements*, Gulf Pub. Co., Houston, 1994.

29. G. C.-Y. Chan, Z. Zhu and G. M. Hieftje, *Spectrochimica Acta Part B: Atomic Spectroscopy*, 2012, **76**, 77-86.

30. K.-S. Ho, K.-O. Lui, K.-H. Lee and W.-T. Chan, *Spectrochimica Acta Part B: Atomic Spectroscopy*, 2013, **89**, 30-39.

31. J. W. Olesik, J. A. Kinzer and G. J. McGowan, *Applied Spectroscopy*, 1997, **51**, 607-616.

32. L. de Galan, R. Smith and J. D. Winefordner, *Spectrochimica Acta Part B-Atomic Spectroscopy*, 1968, **23**, 521-525.

33. R. S. Houk and Y. Zhai, *Spectrochimica Acta Part B-Atomic Spectroscopy*, 2001, **56**, 1055-1067.

34. P. J. Worsfold, A. Townshend and C. F. Poole, eds., *Encyclopedia of analytical science*, Elsevier Academic Press, Oxford, 2005.

35. H. Lindner, A. Murtazin, S. Groh, K. Niemax and A. Bogaerts, *Analytical Chemistry*, 2011, **83**, 9260-9266.

36. H. R. Kuhn, M. Guillong and D. Gunther, *Analytical and Bioanalytical Chemistry*, 2004, **378**, 1069-1074.

37. Z. K. Wang, B. Hattendorf and D. Gunther, *Journal of Analytical Atomic Spectrometry*, 2006, **21**, 1143-1151.

38. L. Flamigni, J. Koch, H. Wiltsche, R. Brogioli, S. Gschwind and D. Gunther, *Journal of Analytical Atomic Spectrometry*, 2012, **27**, 619-625.

39. J. W. Olesik and J. A. Kinzer, *Spectrochimica Acta Part B-Atomic Spectroscopy*, 2006, **61**, 696-704.

40. S. Groh, C. C. Garcia, A. Murtazin, V. Horvatic and K. Niemax, *Spectrochimica Acta Part B-Atomic Spectroscopy*, 2009, **64**, 247-254.

41. G. C.-Y. Chan, Z. Zhu and G. M. Hieftje, *Spectrochimica Acta Part B: Atomic Spectroscopy*, 2012, **76**, 87-95.

42. A. Murtazin, S. Groh and K. Niemax, *Spectrochimica Acta Part B-Atomic Spectroscopy*, 2012, **67**, 3-16.

43. M. H.-P. Yau and W.-T. Chan, *Journal of Analytical Atomic Spectrometry*, 2005, **20**, 1197-1202.

44. K.-S. Ho and W.-T. Chan, *Journal of Analytical Atomic Spectrometry*, 2010, **25**, 1114-1122.

45. C.-N. Tsang, K.-S. Ho, H. Sun and W.-T. Chan, *Journal of the American Chemical Society*, 2011, **133**, 7355-7357.

46. W.-W. Lee and W.-T. Chan, *Journal of Analytical Atomic Spectrometry*, 2015, **30**, 1245-1254.

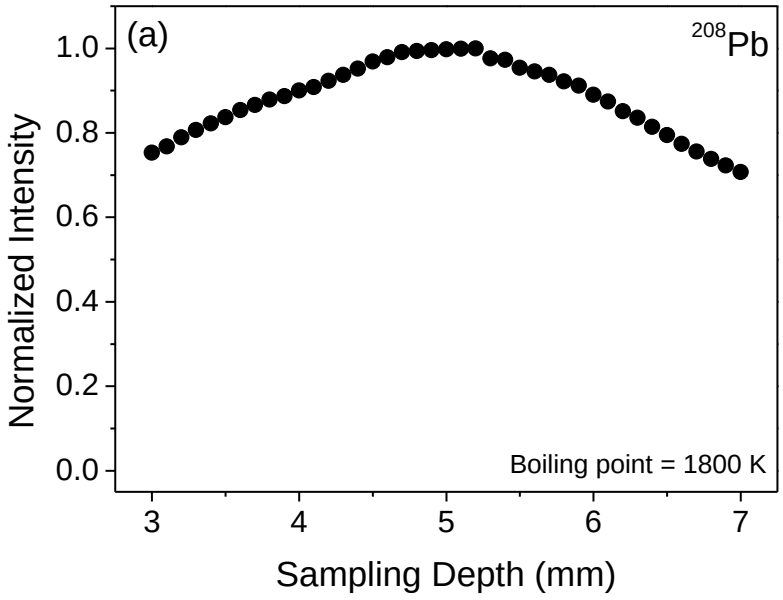

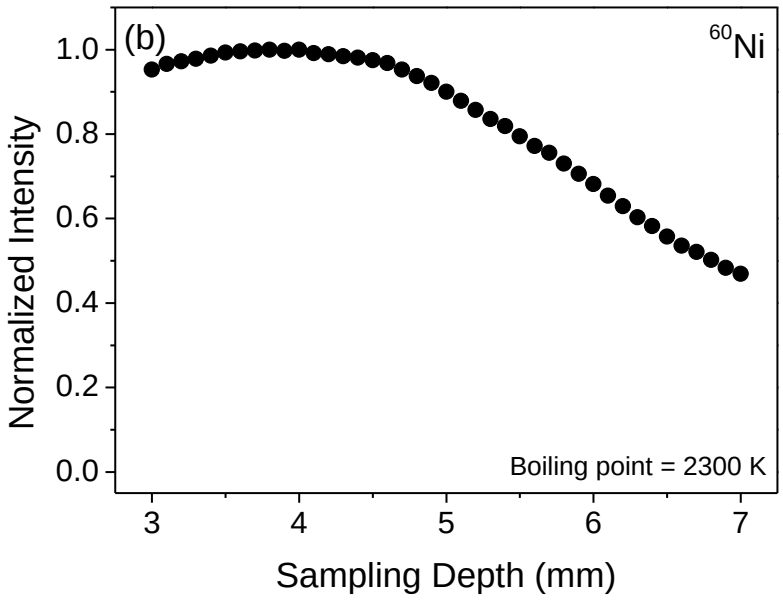

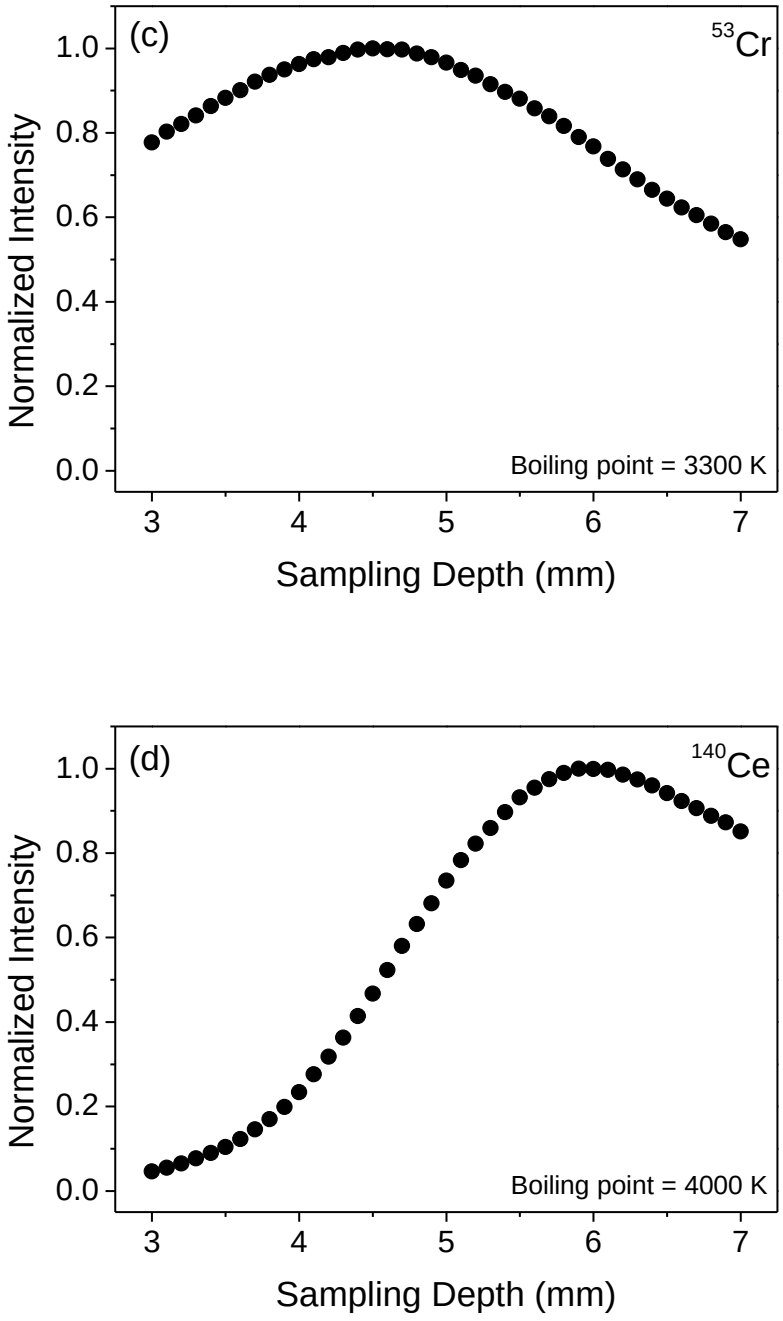

Figure 1. Sampling depth profiles of 4 representative elements. The oxide boiling points of the elements are given in the respective figures.

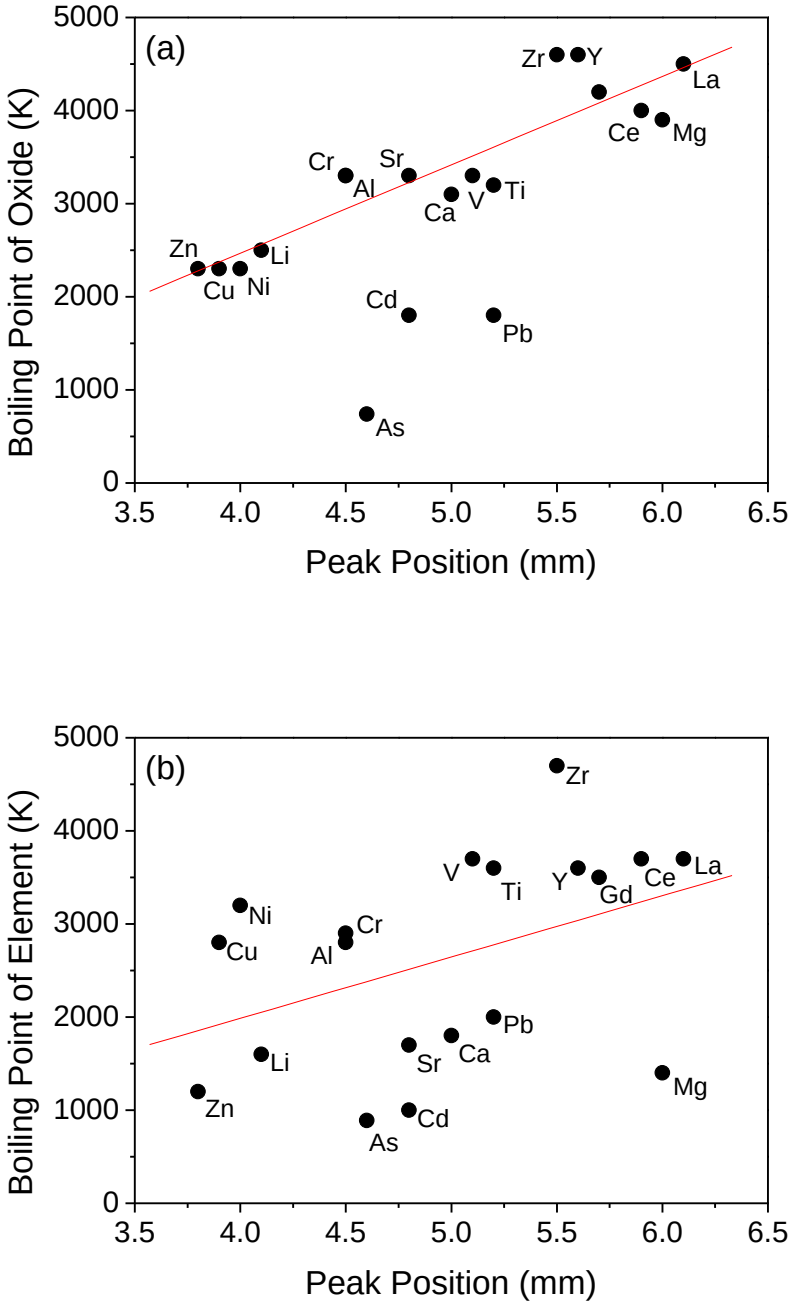

Figure 2. Boiling point of the (a) oxides and (b) elements *versus* the peak position of the ICP-MS sampling depth profile.

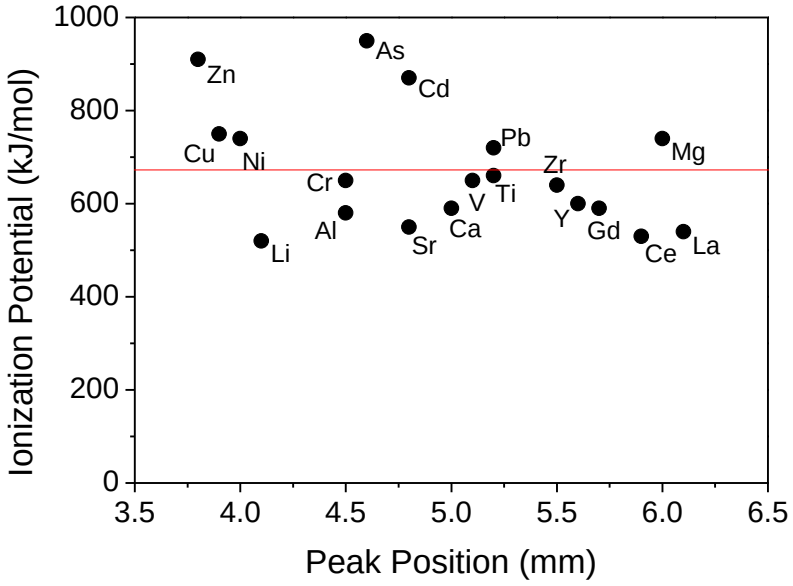

Figure 3. Ionization potential of the elements *versus* the peak position of the ICP-MS sampling depth profile.

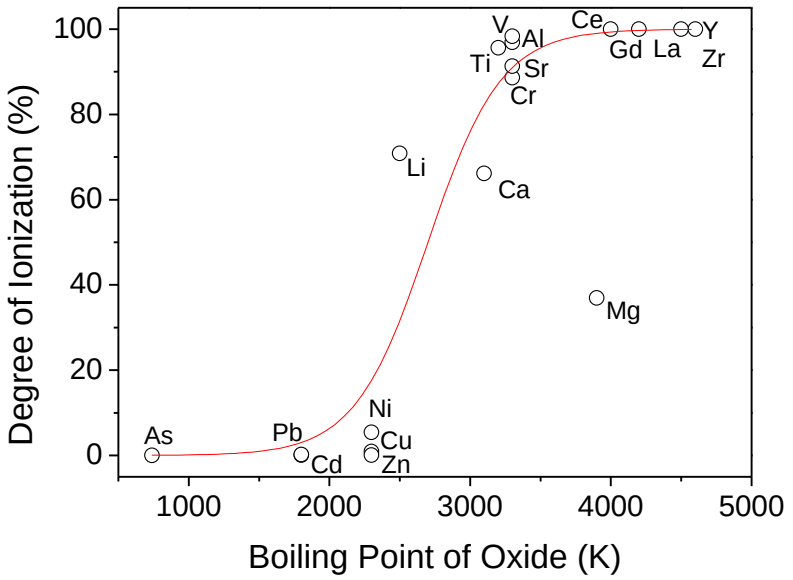

Figure 4. Degree of ionization of the 19 selected elements at the boiling point of the corresponding oxide.

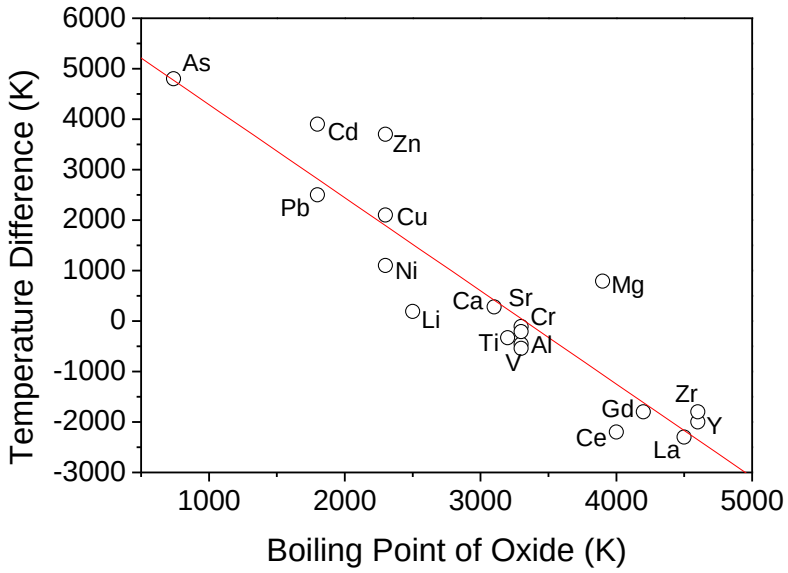

Figure 5. Difference in the temperature for 80% ionization of the elements and the boiling point of the corresponding oxide *versus* the oxide boiling point.

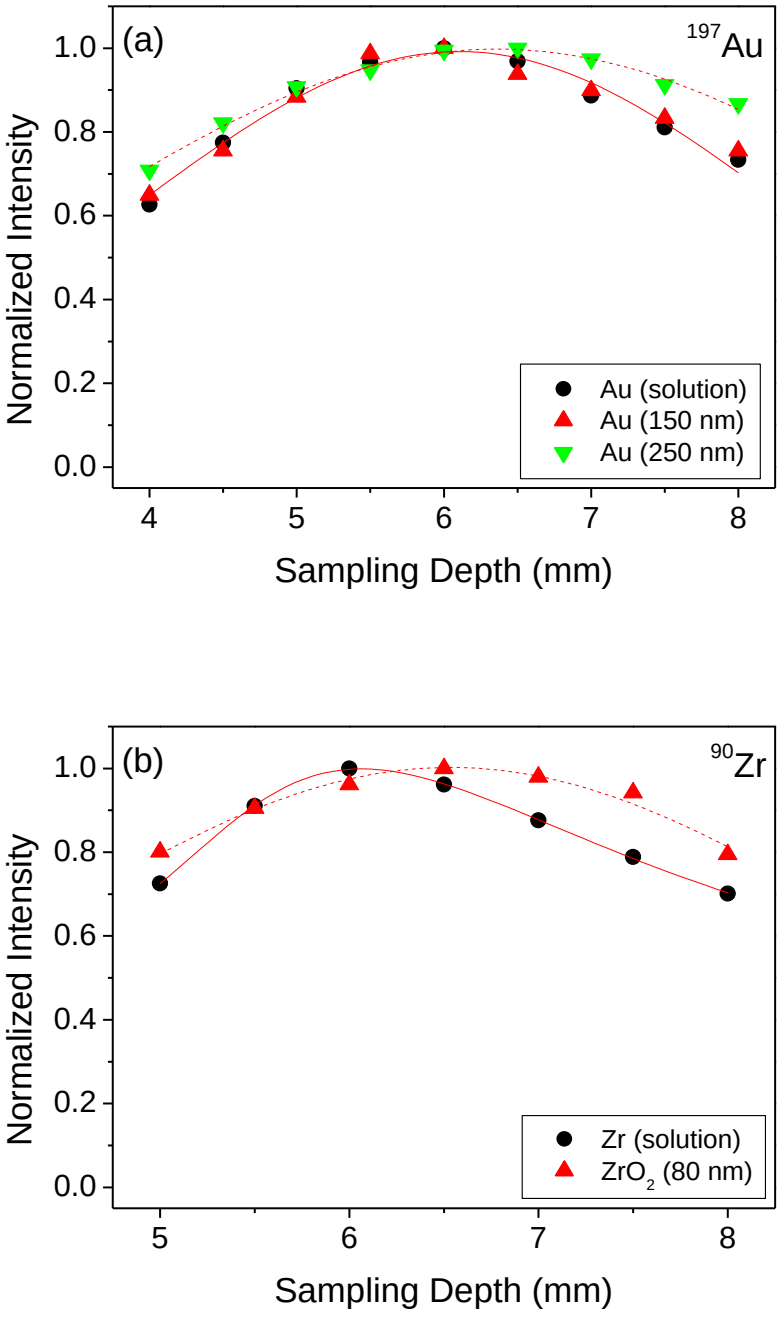

Figure 6. Sampling depth profiles of (a) Au and (b) Zr in the form of aqueous solution of concentration of 10 µg/L and discrete nanoparticles.

Table 1. Properties of the 19 selected elements [20-22].

Element	Monitored m/z ratio	Isotope abundance (%)	Ionization energy (kJ/mol)	Boiling point of element (K)	Oxide species	Oxide bond energy (kJ/mol)	Boiling point of oxide (K)
Li	7	92.41	520	1600	**Li_2O**	330	2500
Mg	25	10.00	740	1400	**MgO**	360	3900
Al	27	100.00	580	2800	**Al_2O_3**	510	3300
Ca	43	0.14	590	1800	**CaO**	400	3100
Ti	47	7.44	660	3600	**TiO_2**	670	3200
V	51	99.75	650	3700	**V_2O_3**	630	3300
Cr	53	9.50	650	2900	**Cr_2O_3**	430	3300
Ni	60	26.22	740	3200	**NiO**	380	2300
Cu	65	69.17	750	2800	**CuO**	270	2300
Zn	66	27.90	910	1200	**ZnO**	160	2300
As	75	100.00	950	890	**As_2O_3**	480	740
Sr	88	82.58	550	1700	**SrO**	430	3300
Y	89	100.00	600	3600	**Y_2O_3**	720	4600
Zr	90	51.45	640	4700	**ZrO_2**	780	4600
Cd	111	12.80	870	1000	**CdO**	240	1800
La	139	99.91	540	3700	**La_2O_3**	800	4500
Ce	140	88.45	530	3700	**Ce_2O_3**	800	4000
Gd	157	15.65	590	3500	**Gd_2O_3**	720	4200
Pb	208	52.40	720	2000	**PbO**	380	1800

Table 2. Operating parameters of ICP-MS and SP-ICP-MS.

	ICP-MS	SP-ICP-MS
Forward power	1200 W	1400 W
Reflected power	<5 W	<5 W
RF frequency	27.12 MHz	27.12 MHz
Plasma gas flow rate (Ar)	15 L/min	15 L/min
Auxiliary gas flow rate (Ar)	1 L/min	1 L/min
Central channel gas flow rate (Ar)	1.25 L/min	1.05 L/min
Type of nebulizer	V-groove	V-groove
Spray chamber	Scott-type double pass (2 ^{o}C)	Scott-type double pass (2 ^{o}C)
Sampling depth	3.0 – 7.0 mm	4.0 – 8.0 mm
Sampler aperture	1.0 mm	1.0 mm
Skimmer aperture	0.4 mm	0.4 mm
ICP torch injector diameter	2.5 mm	1.5 mm
Sample uptake rate	0.40 mL/min	0.40 mL/min
Data acquisition mode	Spectrum mode	Time-resolved analysis
Dwell time	100 ms	10 ms
Replicate	3	--
Measurement duration	--	60 s

Table 3. Peak position of the sampling depth profile *versus* diameter of the dried aerosols.

Concentration of Ce (µg/L)	Calculated diameter of Ce_2O_3 (nm)*	Peak position (mm alc)
1	1.1	5.9
10	2.5	5.9
100	5.3	5.9
1000	11.5	6.0
10000	24.7	5.9

*The average diameter of the aerosols is taken to be 2 µm and the Ce_2O_3 particles are assumed to be spherical in shape of density of 6.20 g/cm^3.

Table 4. Peak position of the sampling depth profiles of the 19 selected elements.

Element	Oxide boiling point (K)	Peak position (mm alc)
As	740	4.6
Cd	1800	4.8
Pb	1800	5.2
Zn	2300	3.8
Cu	2300	3.9
Ni	2300	4.0
Li	2500	4.1
Ca	3100	5.0
Ti	3200	5.2
Al	3300	4.5
Cr	3300	4.5
Sr	3300	4.8
V	3300	5.1
Mg	3900	6.0
Ce	4000	5.9
Gd	4200	5.7
La	4500	6.1
Zr	4600	5.5
Y	4600	5.6